GMR
The Original

SYNTHESIS, CHARACTERIZATION, AND BIOLOGICAL EVALUATION OF GOLD NANOPARTICLES AND GRAPHENE NANOFIBERS WITH AN AUNP–GNF COMPOSITE FOR ANTIBACTERIAL APPLICATION

Preeti Kumari[1], Tulsi Kumar[2], Rohit Sain[3], Sheetal Chawria[4], Minakshi Sharma*[5]

[1,3,4]Department of Zoology, Maharshi Dayanand University, Rohtak (124001), Haryana, India
[2]Department of Microbiology, Maharshi Dayanand University, Rohtak (124001), Haryana, India
[5*]Department of Zoology, Maharshi Dayanand University, Rohtak (124001), Haryana, India, email id: sminakshi.2007@rediffmail.com, ORCID ID - 0000-0003-2926-9671

ABSTRACT

The increasing prevalence of multidrug-resistant bacterial infections has accelerated the development of multifunctional nanomaterials with high efficacy of antimicrobial activity and stability of physicochemical properties. This study synthesized citrate-stabilized gold nanoparticles (AuNPs) via citrate reduction, fabricated graphene nanofibers (GNFs) by electrospinning polyacrylonitrile with reduced graphene oxide (prepared via the modified Hummers' method), and developed an AuNP-GNF composite. The materials were characterized and evaluated for antibacterial activity to determine the zone of inhibition, and antioxidant capacity of the AuNPs was determined. Characterization by UV - spectroscopy, zeta potential analysis, high-resolution transmission electron microscopy (HR-TEM), Fourier transform infrared spectroscopy, and field emission scanning electron microscopy (FESEM) confirmed successful synthesis of the nanomaterials. From the surface plasmon resonance band, AuNPs showed the characteristic band at 540 nm, the zeta potential was −28.0 ± 6.67 mV, and the conductivity was 0.531 mS/cm, which means that the AuNPs were well dispersed in the solution. HR-TEM showed the presence of AuNPs with a mostly spherical shape and good dispersion while FESEM showed continuous bead free GNFs with uniform shape. FTIR substantiated citrate stabilization of AuNPs and embedding of rGO in the nanofibrous matrix. The antibacterial activity of AuNPs was concentration dependent against *B. subtilis*, *P. aeruginosa*, *E. coli* and *S. aureus*, but the activity of GNFs was very low throughout the concentrations. The AuNP-GNF composite retained effective antibacterial activity against all tested bacteria. Additionally, AuNPs exhibited 53 ± 0.7% DPPH free radical scavenging activity at 100 µg/mL. These results show the potential of the AuNP-GNF composite for antimicrobial coatings, wound dressings, and other infection-control applications.

KEYWORDS: Electrospinning; Citrate reduction; Reduced graphene oxide; Nanocomposite; Antibacterial activity; DPPH assay; Multidrug-resistant bacteria; Nanobiomaterials

INTRODUCTION

The global problem of antimicrobial resistance (AMR) is a growing threat that has undermined the ability to use routine antibiotics for clinical treatment and has made it harder to beat infections and lower death rates from multidrug-resistant pathogens (MDRs) (Murray et al., 2022). This crisis has fueled research and interest in the development of nanotechnology-based antimicrobial platforms that can circumvent the known resistance pathways by non-biochemical means, such as through physicochemical mechanisms (Solanki et al., 2024; Fan et al., 2025). Among such platforms, metallic nanoparticles supported on nanostructured carbon scaffolds have attracted growing attention for their capacity to combine intrinsic bioactivity with enhanced structural stability and surface availability (Gao et al., 2025). To fill this gap, the present study focuses on exploring citrate-stabilized gold nanoparticles (AuNPs) immobilized on electrospun graphene nanofibers (GNFs), which are analyzed for their antibacterial and antioxidant activity.

Despite the fact that antimicrobial resistance has traditionally been a problem in hospitals, there is now a very real threat of AMR running throughout all clinical, veterinary and environmental sectors, with it estimated that 4.95 million people died of bacterial AMR in just one reference year (Murray et al., 2022). While most antibiotics target only a single cellular system, nanomaterials can simultaneously target more than one, which is thought to be beneficial for reducing the emergence of antibiotic resistance; however, some nanomaterials have been shown to select for resistance when exposed under specific conditions (Fan et al., 2025). As a result, the use of metal-, carbon-, and polymer-based nanostructures as additional or alternative components to antibiotics has been investigated and their efficacy is highly dependent on their composition, surface chemistry, and dose (Solanki et al., 2024; Sarma et al., 2024). In this view, pairing of a bioactive metallic material with a high surface area structural support has been shown to be a rational approach to achieve enhanced antimicrobial

activity and material durability, which prompted the use of graphene-based nanofibrous scaffolds with gold nanoparticles in the present study.

The citrate reduction method is the most popular method for the preparation of spherical AuNPs because it is simple and reproducible and produces citrate capped AuNPs that are inherently colloidally stabilized (Frens, 1973; Daniel & Astruc, 2004). These combined properties - localised surface plasmon resonance, high surface area-to-volume ratio, and easily tunable surface chemistry - make these nanoparticles useful in diagnostics, drug delivery, and biosensing applications (Khan et al., 2024; Duman et al., 2024). In addition to these physicochemical benefits, AuNPs have a multipronged antibacterial activity that involves multiple mechanisms that act in parallel, including membrane disruption, induction of oxidative stress, and interference with intracellular targets, which makes it much less likely than with antibiotics to develop a single resistance mutation that will restore viability in bacteria (Gao et al., 2025). Their intrinsic radical-scavenging capacity further extends their relevance to antioxidant and wound-healing applications (Ozcicek, 2025). Nevertheless, the unmodified citrate-stabilised AuNPs are still susceptible to aggregation in physiological media or high ionic strength, which may affect their dispersion, long-term stability, and accessibility to the surface (Niżnik et al., 2024). This limitation underscores the need for a supporting matrix that preserves nanoparticle dispersity while maintaining surface availability for biological interactions.

Electrospinning is a versatile method that can generate continuous, high-surface-area nanofibrous materials with tunable morphology and interconnected porosity, and is currently the most popular method for producing nanofibrous scaffolds from precursors derived from graphene (Ji et al., 2024). In this process, reduced graphene oxide is incorporated into PAN matrix to create composite nanofibers which have a combination of graphene's electrical conductivity and chemical stability with PAN's mechanical properties, spinnability and fibre-forming ability (Wang et al., 2024). This fibrous structure gives rise to large specific surface area, interconnected porosity and many surface active sites, which are conducive to effective anchoring of nanoparticles and interfacial interaction. However, the intrinsic antibacterial activity of fibrous materials based on graphene is often weak, and their biological performance is greatly enhanced when they are functionalised with metallic nanoparticles, not only because they provide further antibacterial mechanisms, but also because they are better dispersed and less prone to aggregation on the fibrous support (Gautam et al., 2024). These considerations are a justification for the choice of the electrospun GNFs as a matrix with a high surface area and mechanical stability to immobilise AuNPs, the composite of which was developed in the present study.

Despite the individual studies on citrate-AuNPs and rGO/PAN nanofibers for their antimicrobial application, the studies involving their combined application in the same nanofiber composite material with simultaneous physicochemical characterization and antimicrobial activity testing against Gram-positive and Gram-negative bacteria are limited. The current AuNP/GO or rGO systems are composed primarily of planar GO/rGO sheets or one-step co-reduction, and most of them do not test for antioxidants despite showing antibacterial effects (Martinov et al., 2025; Asgari et al., 2022). This disparity also hampers the understanding of the special role of the fibrous graphene scaffold in dispersion, stability, and combined bioactivity of AuNPs. This prompted the present study to synthesize citrate stabilised AuNPs, electrospun rGO/PAN GNFs and fabricate AuNP-GNF composite and characterise with UV-Vis spectroscopy, zeta potential analysis, HR-TEM, FTIR and FESEM. The antibacterial activity of the AuNPs, GNFs and composite were tested against *Escherichia coli*, *Pseudomonas aeruginosa*, *Staphylococcus aureus* and *Bacillus subtilis*, whereas the antioxidant activity of AuNPs was determined using the DPPH assay.

2. Experimental Procedures

2.1 Chemicals and reagents

Tetrachloroauric (III) acid trihydrate (HAuCl4.3H2O), graphite flakes, trisodium citrate, polyacrylonitrile (PAN) and sodium nitrate ($NaNO_3$) were purchased from Sigma-Aldrich (St. Louis, MO, USA). Potassium permanganate ($KMnO_4$), Sulfuric acid (H_2SO_4) 98%, ascorbic acid, hydrogen peroxide (H_2O_2) 30%, N, N-dimethylformamide (DMF), ethanol, 2,2-diphenyl-1-picrylhydrazyl (DPPH), nutrient broth (NB), and Mueller–Hinton agar (MHA) were obtained from HiMedia Laboratories Pvt. Ltd. (Mumbai, India). In antimicrobial assays, for positive control kanamycin (50 µg/mL) was used, whereas for negative control, double-distilled water was used. All reagents and chemicals used throughout the experiment were of analytical grade and used without any further purification.

2.2 Apparatus

Ultraviolet–visible (UV–Vis) spectrum was monitored by a UV–Vis spectrophotometer (Malvern Panalytical Ltd., UK) in wavelength ranges from 200–800 nm. The hydrodynamic size as well as zeta potential of the prepared AuNPs were determined by a Zetasizer Nano ZS (Malvern Panalytical Ltd., UK) at 25°C with a scattering angle of 173°. The morphology and particle size of AuNPs were examined using high-resolution transmission electron microscopy (HR-TEM; TECNAI G20, 200 kV, Thermo Scientific). Fourier transform infrared (FTIR) spectra were acquired using a Bruker FTIR spectrometer (Bruker Corporation, Germany) over the spectral range of 4000–500 cm^{-1}. To analyze the surface morphology of graphene nanofibers the field emission scanning electron microscope (FESEM; Carl Zeiss Sigma 360, Germany). Electrospinning was performed via SUPER ES-2 electrospinning unit (E-Spin Nanotech Pvt. Ltd., Kanpur, India). A refrigerated

centrifuge equipment (Genetix Biotech Asia Pvt. Ltd., India) was used during nanoparticle synthesis and purification.

2.3 Microorganisms

The antibacterial activity of the synthesized gold nanoparticles (AuNPs), graphene nanofibers (GNFs), and AuNP–GNF composite was evaluated against four reference bacterial strains: *Pseudomonas aeruginosa* (MTCC 424), *Escherichia coli* (MTCC 443), *Bacillus subtilis* (MTCC 121), and *Staphylococcus aureus* (MTCC 96). All bacterial strains were procured from the Department of Microbiology, Maharshi Dayanand University, Rohtak, Haryana, India. The cultures were maintained at 37°C in nutrient broth (HiMedia Laboratories Pvt. Ltd., Mumbai, India) for 12 hours, and that innoculum density was adjusted to the 0.5 McFarland standard prior to antimicrobial assays.

2.4 Synthesis of gold nanoparticles (AuNPs)

AuNPs were prepared by aqueous auric chloride solution reduction with citrate by following the method of Batra and Pundir (2013), which was based on the classical protocol of Turkevich–Frens (Turkevich et al., 1951; Frens, 1973). In short, 0.01 g of auric chloride was mixed in 100 mL of double-distilled water, under continuous magnetic stirring it is heated to boiling. Subsequently, 2.5 mL trisodium citrate solution of 1% (w/v) was added to the boiled gold salt solution under vigorous stirring. The reaction mixture was kept under boiling conditions until the appearance of the characteristic dark wine-red color, confirming the synthesis of AuNPs. The prepared suspension of AuNP was allowed to cool at room temperature and then stored at 4°C in the dark glass bottle for further characterization and biological evaluation.

2.5 Synthesis of graphene nanofibers (GNFs)

Using reduced graphene oxide (rGO) as the starting material, graphene nanofibers (GNFs) were synthesized. The process has a series of three steps: (i) graphene oxide (GO) preparation by the modified Hummers' method, (ii) chemical reduction of GO to rGO, and (iii) synthesis of GNFs by electrospinning of an rGO/polyacrylonitrile (PAN) solution.

2.5.1 Preparation of graphene oxide (GO)

Graphene oxide (GO) was synthesized using the modified Hummers' method with slight modifications (Hummers and Offeman, 1958; Marcano et al., 2010). 1g of sodium nitrate (NaNO3) and 2g of graphite flakes were added in 17 mL of double-distilled water and subsequently continuous and gradual addition of 33 mL of 98% sulfuric acid (H2SO4) while maintained in an ice-bath. The reaction mixture was magnetically stirred for 15 min, after which 8 g of potassium permanganate ($KMnO_4$) was added slowly while maintaining the temperature at 20°C. Subsequently, 100 mL of double-distilled water was added, and the mixture was stirred at 40°C for 90 min. The reaction was terminated by adding 12 mL of 30% hydrogen peroxide (H_2O_2), giving rise to a brown suspension. Washing of the synthesized suspension was done four to five times with double-distilled water and ethanol, and the obtained GO was dried at 60° for 8h in a hot-air oven.

2.5.2 Preparation of reduced graphene oxide (rGO)

Reduced graphene oxide (rGO) was prepared by the chemical reduction of graphene oxide (GO) using L-ascorbic acid and trisodium citrate, following a modified procedure reported in the literature (Fernández-Merino et al., 2010; Pei and Cheng, 2012). Briefly, 50 mg of GO was dispersed in 50 mL of double-distilled water and sonicated for 4 h at a temperature below 60°C. Briefly, 50 mg of GO was mixed in 50 mL of double-distilled water and sonicated for 4 h at a temperature below 60°C. Subsequently, 40 mg of trisodium citrate and 80 mg of L-ascorbic acid were added, and the mixture was magnetically stirred at room temperature for 48 h. Washing of the formed rGO suspension was done three to four times with ethanol and double-distilled water and dried at 60°C for 8 h in a hot-air oven.

2.5.3 Synthesis of graphene nanofibers (GNFs)

Graphene nanofibers (GNFs) were synthesized by the electrospinning technique using reduced graphene oxide (rGO) and polyacrylonitrile (PAN), following a modified procedure described previously (Ji et al., 2024; Kumari and Sharma, 2025). Briefly, 0.01 g of rGO was dispersed in 20 mL of N, N-dimethylformamide (DMF) and sonicated for 2 h. Subsequently, 2 g of PAN was added, and the mixture was maintained at stirring for 12 h to obtain a homogeneous electrospinning solution. The syringe was filled with 5 mL of solution, and electrospinning was performed using an electrospinning unit with a 10 cm needle-to-collector distance, a 0.5 mL h^{-1} solution flow rate, and an applied voltage of 11 kV. Clean aluminum foil was placed over the collector to collect the electrospun nanofibers. The synthesized GNFs were subsequently characterized by Fourier transform infrared (FTIR) spectroscopy and field emission scanning electron microscopy (FESEM).

Characterization of gold nanoparticles (AuNPs)

The synthesized gold nanoparticles were characterized to evaluate their optical, surface, morphological, and chemical properties using ultraviolet–visible (UV–Vis) spectroscopy, zeta potential analysis, high-resolution

transmission electron microscopy (HR-TEM), and Fourier transform infrared (FTIR) spectroscopy. The analytical procedures employed for each characterization technique are described in the following subsections.

2.5.4 Ultraviolet–visible (UV–Vis) spectroscopy

Analysis of the optical properties of the gold nanoparticles (AuNPs) was performed using a UV–Vis spectrophotometer (Malvern Panalytical Ltd., UK). Prior to analysis, the AuNP suspension was sonicated for 10 min to obtain a homogeneous dispersion. The sample was transferred to a thoroughly cleaned 1 cm path-length quartz cuvette, and the absorbance spectrum was recorded over the wavelength range of 400–700 nm using double-distilled water as the blank. The obtained spectra were used for subsequent analysis of the prepared AuNPs.

2.5.5 Zeta potential analysis

The zeta potential of the synthesized gold nanoparticles (AuNPs) was analyzed using a Zetasizer Nano ZS (Malvern Panalytical Ltd., UK) at 25°C with a 173° backscatter detection angle. The AuNP suspension was analyzed immediately after synthesis, and measurements were conducted according to the manufacturer's operating instructions to evaluate the nanoparticles' surface charge (Bhattacharjee, 2016).

2.5.6 High-resolution transmission electron microscopy (HR-TEM)

The morphology and particle size of the synthesized gold nanoparticles (AuNPs) were examined using high-resolution transmission electron microscopy (HR-TEM; TECNAI G20, 200 kV, Thermo Scientific). Onto a carbon-coated copper grid, a drop of the AuNP suspension was placed and allowed to dry under ambient conditions prior to imaging. Micrographs were acquired at an accelerating voltage of 200 kV, and the obtained images were used to evaluate the morphology and size distribution of the synthesized AuNPs (Li et al., 2024).

2.5.7 Fourier transform infrared (FTIR) spectroscopy of AuNPs

Functional groups present on the surface of the synthesized gold nanoparticles (AuNPs) were identified by a Fourier transform infrared (FTIR) spectrometer (Bruker Corporation, Germany). FTIR spectra were taken within the range of 4000-500 cm^{-1} and the obtained spectra were used to identify the functional groups responsible for citrate capping and stabilizing of the synthesized AuNPs (Pasieczna-Patkowska et al., 2025; Li et al., 2024).

2.6 Characterization of graphene nanofibers (GNFs)

The synthesized graphene nanofibers (GNFs) were characterized to evaluate their surface morphology and chemical functional groups using field emission scanning electron microscopy (FESEM) and Fourier transform infrared (FTIR) spectroscopy. FESEM was employed to examine the morphology, fiber continuity, and surface characteristics of the electrospun nanofibers, whereas FTIR spectroscopy was performed to identify the characteristic functional groups and confirm the incorporation of reduced graphene oxide within the polyacrylonitrile nanofibrous matrix. The analytical procedures are described in the following subsections.

2.6.1 Field emission scanning electron microscopy (FESEM)

The surface morphology of the synthesized graphene nanofibers (GNFs) was examined using a field emission scanning electron microscope (FESEM; Carl Zeiss Sigma 360, Germany). A representative specimen of the electrospun GNF mat was mounted on the specimen holder, and the surface morphology was analyzed at EHT 5kV, magnification 5Kx, and using the SE1 detector. The acquired micrographs were used for subsequent morphological analysis of the synthesized GNFs.

2.6.2 Fourier transform infrared (FTIR) spectroscopy of graphene nanofibers

The functional groups of the synthesized graphene nanofibers (GNFs) were characterized using a Fourier transform infrared (FTIR) spectrometer (Bruker Corporation, Germany). FTIR spectra were recorded over the spectral range of 4000–500 cm^{-1}, and the acquired spectra were used for the identification of the characteristic functional groups present in the synthesized GNFs.

2.7 Antimicrobial activity

The antibacterial activities of the synthesized gold nanoparticles (AuNPs), graphene nanofibers (GNFs), and AuNP–GNF composite were evaluated against four reference bacterial strains, namely *Escherichia coli* (MTCC 443), *Pseudomonas aeruginosa* (MTCC 424), *Staphylococcus aureus* (MTCC 96), and *Bacillus subtilis* (MTCC 121). Fresh bacterial cultures were prepared in nutrient broth (HiMedia Laboratories Pvt. Ltd., Mumbai, India) and incubated at 37°C for 12 h. The bacterial inocula were adjusted to the 0.5 McFarland turbidity standard before antimicrobial assays. All experiments were performed in triplicate using standard agar diffusion procedures. (Balouiri et al., 2016; Chung et al., 2023).

2.7.1 Antibacterial activity of gold nanoparticles (AuNPs)

The antibacterial activity of AuNPs was determined using the agar well diffusion method. The standardized

bacterial suspension was consistently added to Mueller-Hinton agar (MHA) plates. 8 mm-diameter wells were prepared using a sterile cork borer. Subsequently, 100 µL of AuNP suspension at concentrations of 100%, 75%, 50%, and 25% was dispensed into the wells. Kanamycin (50 µg/mL) was used as the positive control, whereas double-distilled water served as the negative control. The culture medium plates were incubated at 37°C, and the antibacterial activity was determined by measuring the diameter of the inhibition zones. All experiments were performed in triplicate.

2.7.2 Antibacterial activity of graphene nanofibers (GNFs) and AuNP–GNF composite

The antibacterial activity of graphene nanofibers (GNFs) and the AuNP–GNF composite was evaluated against the selected bacterial strains using a modified agar diffusion method. Sterile Mueller–Hinton agar (MHA) plates were uniformly inoculated with the standardized bacterial suspension. For GNF evaluation, a single sterile 8 mm GNF disc was placed on the surface of the inoculated agar. For the AuNP–GNF composite, an 8 mm-diameter well was prepared in the agar, into which one UV- sterilized GNF disc was carefully placed, followed by the addition of 100 µL of a 100% AuNP suspension to form the composite. Kanamycin (50 µg/mL) was used as the positive control. The plates were incubated at 37°C, and the inhibitory zone was measured to determine the antibacterial activity. All experiments were performed in triplicate.

2.8 DPPH free radical scavenging assay

The antioxidant activity of the synthesized gold nanoparticles (AuNPs) was estimated by using the 2,2-diphenyl-1-picrylhydrazyl (DPPH) free radical scavenging assay with slight modifications of the method described by Brand-Williams et al. (1995). Briefly, 100 µg/mL AuNP suspension was mixed with a freshly prepared 0.1 mM DPPH solution in methanol, vortexed thoroughly, and incubated in the absence of light at room temperature for 30 min. Ascorbic acid was prepared as the positive control, while the DPPH solution without AuNPs served as the control. After incubation, the absorbance was measured at 517 nm using a UV–Vis spectrophotometer. All measurements were performed in triplicate, and the percentage of DPPH radical scavenging activity was calculated using the following equation:

$$\text{DPPH radical scavenging activity (\%)} = \frac{Ac - As}{Ac} \times 100$$

where Ac represents the absorbance of the control and As represents the absorbance of the sample. This protocol is consistent with recent AuNP antioxidant studies employing the DPPH assay.

2.9 Statistical analysis

The data are shown as mean ± standard deviation (SD), and each experiment was conducted in triplicate.

3. RESULTS AND DISCUSSION

3.1 Ultraviolet-visible (UV-Vis) spectroscopy of AuNPs

The UV-Vis spectrum of synthesized gold nanoparticles (AuNPs) showed a strong absorption peak at 540 nm, which was typical of a gold nanoparticle solution (Fig. 1a), confirming the successful formation of colloidal AuNPs. The absorption band is a characteristic band of AuNPs that is caused by the collective oscillation of the conduction electrons when interacting with the incident light, known as localized surface plasmon resonance (LSPR).

The observed SPR peak is in the range of the characteristic absorption peak of chemically synthesized citrate-stabilized AuNPs and comparable to the recent studies that reported the SPR peak to be in the range 520-550 nm for predominantly spherical AuNPs (Zhang et al., 2025). The position of the SPR is typically dependent on the size, shape, aggregation, surface chemistry, and refractive index of the surrounding medium of the nanoparticles (Raguindin and Mercado, 2023). The absorption maximum in the present study is therefore the characteristic absorption of a successful synthesis of nanoparticles, and confirms the HR-TEM observation of mostly spherical AuNPs.

Overall, the successful synthesis of AuNPs appropriate for the further physicochemical characterization and biological testing was corroborated by the UV-Vis analysis, in addition to the characteristic wine-red colour observed during the synthesis process.

3.2 Zeta potential analysis of AuNPs

The synthesized AuNPs showed a zeta potential of −28.0 mV, zeta deviation of 6.67 mV, and a conductivity of 0.531 mS/cm (Fig. 1b), which suggested that the AuNPs had good colloidal stability and a negatively charged surface. The negative surface charge is thought to be due to citrate adsorption during synthesis of the nanoparticles, which provides electrostatic repulsion and prevents aggregation. Citrate capped AuNPs with zeta potential between −20 and −30 mV are generally considered to have a stable dispersion (Bhattacharjee, 2016; Duman et al., 2024). The relatively low conductivity (0.531 mS/cm) further suggests a low ionic-strength dispersion, which favors electrostatic stabilization of the nanoparticles. Similar zeta potential values (−24 to −33 mV) have recently been reported for chemically synthesized AuNPs exhibiting good colloidal stability and reproducible physicochemical properties (Kumari and Sharma, 2025; Wang et al., 2014). In conclusion, the

synthesized AuNPs were found to have adequate electrostatic stability as confirmed by the zeta potential analysis and could be further characterized and used for biological evaluation purposes

3.3 High-resolution transmission electron microscopy (HR-TEM) of AuNPs

The HR-TEM micrograph confirmed the successful formation of mostly spherical AuNPs with well dispersion throughout the field of view, although small localized aggregates were observed in a small number of areas (Fig. 1c). The majority of spherical nanoparticles is consistent with the characteristic surface plasmon resonance (SPR) band observed at 540 nm in the UV-Vis spectrum (Fig. 1a), supporting the successful synthesis of AuNPs via the citrate reduction method. Chemically synthesized AuNPs with citrate-caps showed similar shapes with nanoparticles being spherical with minimal aggregation, which was claimed to be due to effective surface stabilization by citrate (Li et al., 2024).

The localized aggregation seen in the present study is similar to that presented in the previous studies and could be due to partial particle-particle interactions, during sample drying on the TEM grid, and does not necessarily mean that extensive aggregation occurs within the colloidal suspension (Raguindin and Mercado, 2023). In general, the HR-TEM results supported the UV-Vis and zeta potential data, indicating that the AuNPs were successfully synthesized with predominantly spherical morphology and that their morphological uniformity was satisfactory for further biological studies.

3.4 Fourier transform infrared (FTIR) spectroscopy of AuNPs

The synthesized AuNPs showed absorption bands at 3260.91, 2140.67, and 1639.83 cm^{-1} in its FTIR spectrum (Fig. 1d). The broad absorption band at 3260.91 cm^{-1} corresponds to O-H stretching vibrations, indicating the presence of hydroxyl groups, whereas the band at 1639.83 cm^{-1} is attributed to the carboxylate ($-COO^-$) stretching vibration of citrate molecules adsorbed on the AuNP surface. 2140.67 cm^{-1}, the weak band is considered a minor vibrational feature and not assigned to a specific functional group. The hydroxyl and carboxylate functional groups confirm the presence of citrate on the surface of the nanoparticles, which act as capping agent and stabilize the nanoparticles and prevent their aggregation by electrostatic repulsion. The FTIR spectral shapes are comparable for citrate mediated AuNPs, indicating that citrate is an important surface stabilizer of AuNPs and also serves to maintain the dispersion of nanoparticles (Pasieczna-Patkowska et al., 2025; Li et al., 2024). These findings are consistent with the negative zeta potential (−28.0 mV) observed in the present study, confirming the successful synthesis and stabilization of AuNPs.

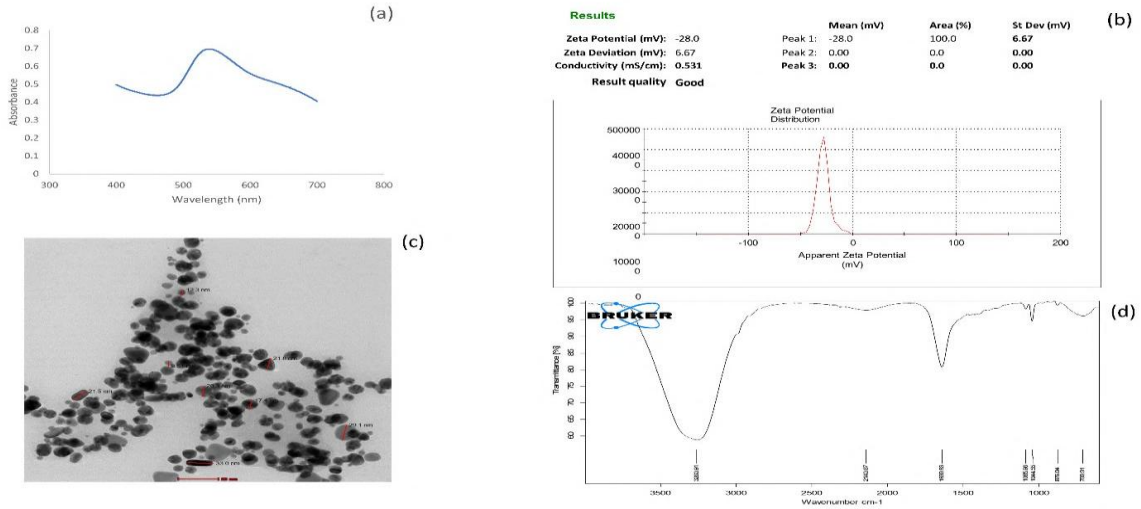

Figure 1. Physicochemical characterization of the chemically synthesized gold nanoparticles (AuNPs). (a) An ultraviolet-visible (UV-Vis) absorption spectrum exhibiting characteristic localized surface plasmon resonance (LSPR) band of AuNPs. (b) Zeta potential profile showing surface charge and colloidal stability of AuNPs synthesized. (c) High-resolution transmission electron microscopy (HR-TEM) micrograph showing the morphology and dispersion of AuNPs. (d) FTIR spectrum of citrate-capped AuNPs displaying the characteristic functional groups associated with citrate-capped AuNPs.

3.5 Field emission scanning electron microscopy (FESEM) of graphene nanofibers (GNFs)

The FESEM micrograph (Fig. 2a) verified the successful fabrication of electrospun graphene nanofibers (GNFs) in the form of a continuous, randomly oriented fibrous network. The nanofibers exhibited a smooth surface morphology, relatively uniform fiber diameter, and no evident bead formation or structural defects within the observed field, showing stable electrospinning and homogeneous dispersion of the rGO/PAN precursor solution. The observed morphology aligns with recent reports on optimizing electrospinning parameters for the formation of uniform and bead-free nanofibers from graphene materials that exhibit structural integrity and porous

architectures. This continuous fibrous network offers excellent surface-to-volume ratio and abundant surface active sites that are beneficial for subsequent loading of AuNPs and could allow interactions with bacterial cells in antimicrobial applications (Ji et al., 2024; Asgari et al., 2022). As a whole, the FESEM analysis confirmed the successful fabrication of morphologically uniform GNFs that could be used to form the composites and further subjected to biological evaluation.

3.6 Fourier transform infrared (FTIR) spectroscopy of graphene nanofibers (GNFs)

FTIR spectrum of the synthesized GNFs exhibited absorption bands at 3741.38, 2934.38, 2368.04, 1697.42, and 1523.13 cm^{-1} (Fig. 2b). The broad band at 3741.38 cm^{-1} corresponds to O-H stretching, indicating the presence of oxygen-containing functional groups, while the peak at 2934.38 cm^{-1} is aliphatic C-H stretching. The absorption band at 2368.04 cm^{-1} is attributed to the C≡N stretching of polyacrylonitrile (PAN), whereas the peaks at 1697.42 and 1523.13 cm^{-1} correspond to C=O stretching and N-O asymmetric stretching, respectively. The characteristic functional groups verify the successful incorporation of rGO into the PAN nanofibers matrix, similar to previous reports on electrospun graphene-based nanofibers. The presence of both oxygen and nitrogen groups creates active surface functional groups that enable the immobilization of AuNPs and help stabilize the structure of the nanofibers, which are compatible with their future use in antimicrobial applications (Ji et al., 2024; Gautam et al., 2024).

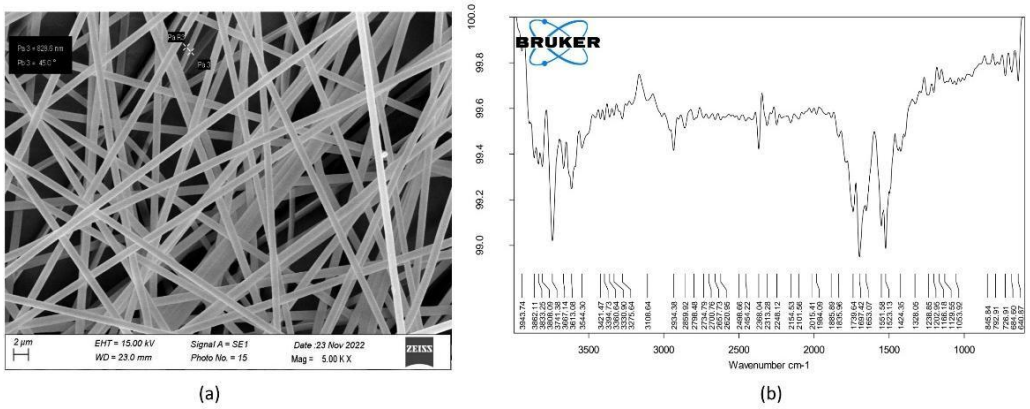

Figure 2. Physicochemical characterization of electrospun graphene nanofibers (GNFs): (a) Field emission scanning electron microscopy (FESEM) micrograph showing the surface morphology of GNFs; (b) Fourier transform infrared (FTIR) spectrum showing the characteristic functional groups of GNFs.

3.7.1 Antibacterial activity of AuNPs

Antibacterial activity of the synthesized AuNPs was tested against *Pseudomonas aeruginosa* (MTCC 424), *Escherichia coli* (MTCC 443), *Staphylococcus aureus* (MTCC 96), and *Bacillus subtilis* (MTCC 121) using the agar well diffusion assay (Fig. 3; Table 1). The antibacterial activity of the AuNPs was concentration dependent with the inhibition zone (ZOI) increasing gradually with the increasing concentration of AuNPs for all the bacteria used.

At 100% AuNP concentration, the highest antibacterial activity was observed against *B. subtilis* (15 ± 0.1 mm), followed by *P. aeruginosa* (14 ± 0.6 mm), whereas *E. coli* and *S. aureus* exhibited comparable inhibition zones (13 ± 0.1 and 13 ± 0.4 mm, respectively). A gradual reduction in antibacterial activity was observed with decreasing AuNP concentrations. At 25%, the inhibition zones decreased to 11 ± 0.4 mm for *B. subtilis* and 9 ± 0.3-0.9 mm for the remaining bacterial strains. Although the antibacterial activity of AuNPs was lower than that of kanamycin (25-28 mm), appreciable growth inhibition was observed against both Gram-positive and Gram-negative bacteria (Table 1).

Table 1. Concentration-dependent antibacterial activity of chemically synthesized gold nanoparticles (AuNPs) against Gram-negative and Gram-positive bacterial strains determined by the agar well diffusion assay.

Bacterial strain (MTCC)	Zone of inhibition (mm, mean ± SD, n=3)				Positive control
	AuNPs (100%)	AuNPs (75%)	AuNPs (50%)	AuNPs (25%)	Kanamycin (50 µg/mL)

***P. aeruginosa* (424)**	14±0.6	13±0.1	11±0.8	9±0.3	25±0.5
***E. coli* (443)**	13±0.1	11±0.3	10±0.5	9±0.6	26±0.2
***Staphylococcus aureus* (96)**	13±0.4	11±0.6	10±0.5	9±0.9	25±0.9
***Bacillus subtilis* (121)**	15±0.1	14±0.7	12±0.1	11±0.4	28±0.8

Concentration dependent antibacterial activity was observed, which aligns with the previously reported observations that higher concentration of AuNP in the medium increases the interaction of AuNP with the bacteria, contributing to the damage of the cell membrane, oxidative stress and disruption of essential cellular functions (Duman et al., 2024; Cui et al., 2012). The significant effect of citrate capped AuNPs on *B. subtilis* in the present study corroborates with recent reports demonstrating effective antimicrobial activity against Gram-positive bacteria and the inhibition of *E. coli* and *P. aeruginosa* further exemplifying the broad spectrum antibacterial potential of AuNPs (Duman et al., 2024).

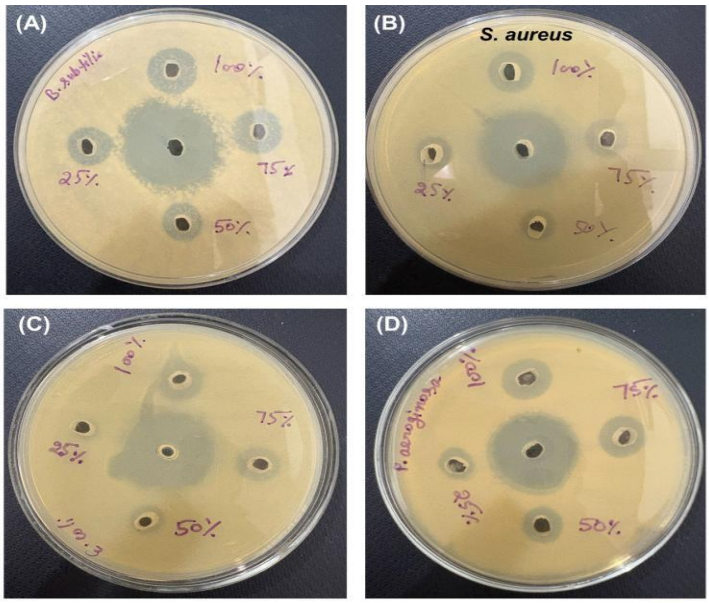

Figure 3. The concentration-dependent antibacterial activity of chemically synthesized gold nanoparticles (AuNPs) against Gram-negative and Gram-positive bacterial strains by agar well diffusion assay.
Representative agar plates showing the zones of inhibition produced by AuNPs at 25%, 50%, 75%, and 100% concentrations against (a) *Escherichia coli* (MTCC 443), (b) *Pseudomonas aeruginosa* (MTCC 424), (c) *Staphylococcus aureus* (MTCC 96), and
(d) *Bacillus subtilis* (MTCC 121), with kanamycin (50 µg/mL) as the positive control.

3.7.2 Comparative antibacterial activity of graphene nanofibers (GNFs) and AuNP-GNF composite

The antibacterial activities of GNFs and the AuNP-GNF composite against *Pseudomonas aeruginosa* (MTCC 424), *Escherichia coli* (MTCC 443), *Staphylococcus aureus* (MTCC 96), and *Bacillus subtilis* (MTCC 121) are presented in Fig. 4 and Table 2. The GNF disc alone exhibited negligible antibacterial activity, producing inhibition zones of 0-0.5 mm against all tested bacteria. In contrast, the AuNP-GNF composite showed pronounced antibacterial activity, with inhibition zones of 14 ± 0.6 mm against *P. aeruginosa*, 13 ± 0.5 mm against *E. coli*, 13 ± 0.7 mm against *S. aureus*, and 15 ± 0.4 mm against *B. subtilis*. Although kanamycin produced the largest inhibition zones (25-28 mm), the composite effectively inhibited the growth of both Gram-positive and Gram-negative bacteria.

Table 2. Comparative antibacterial activity of graphene nanofibers (GNFs), gold nanoparticles (AuNPs), and the AuNP-GNF composite against Gram-negative and Gram-positive bacterial strains.

Bacterial strain (MTCC)	**Zone of inhibition (mm, mean ± SD, n = 3)**				**Positive control**
	GNF disc	AuNPs (100%)	AuNP-GNF composite	DDW	Kanamycin (50 µg/mL)
***Pseudomonas aeruginosa* (424)**	0.1 - 0.5	14±0.5	14±0.6	–	25±0.4
***E. coli* (443)**	0.1 - 0.5	13±0.4	13±0.5	–	26±0.1
***Staphylococcus aureus* (96)**	0.1 - 0.5	13±0.4	13±0.7	–	25±0.3
***Bacillus subtilis* (121)**	0 .1- 0.5	15±0.2	15±0.4	–	28±0.6

The marked increase in antibacterial activity following AuNP immobilization demonstrates that the GNFs primarily functioned as a supporting matrix, while the antimicrobial activity was predominantly imparted by the surface-bound AuNPs. The nanofibrous architecture provides a large surface area for uniform nanoparticle distribution and promotes effective contact with bacterial cells, thereby enhancing membrane disruption and oxidative stress (Qin et al., 2024; Ibrahim et al., 2020). Similar antibacterial responses of AuNP-decorated graphene-based nanofibers have been reported in recent studies, highlighting their potential as broad-spectrum antimicrobial materials (Yang et al., 2017).

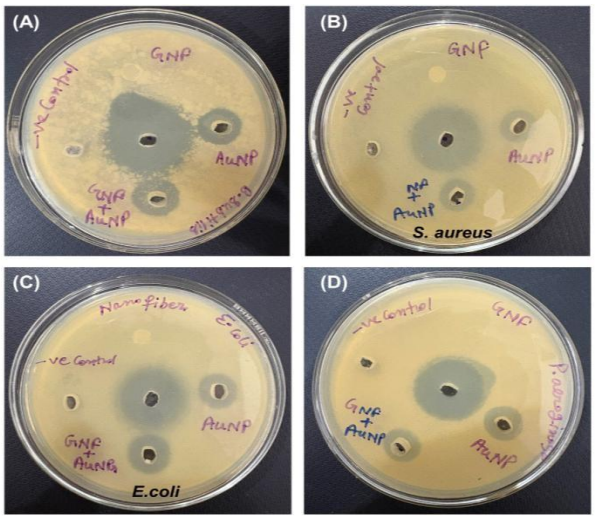

Figure 4. The comparative antibacterial activity of graphene nanofibers (GNFs), gold nanoparticles (AuNPs), and the AuNP-GNF composite against Gram-negative and Gram-positive bacterial strains. The agar plates showing antibacterial activity against (A) *P. aeruginosa* (424), (B) *S. aureus* (96), (C) *E. coli* (443), and (D) *B. subtilis* (121) following treatment with a GNF disc, AuNPs, AuNP-GNF composite, kanamycin (50 µg/mL) as the positive control, and double-distilled water (DDW) as the negative control.

3.7.3 Proposed antibacterial mechanism of the AuNP-GNF composite

The antibacterial activity of the AuNP-GNF composite is proposed to arise from the combined effects of AuNPs and the graphene nanofibrous scaffold (Fig. 5). The electrospun GNFs provide a high-surface-area support for the uniform immobilization and distribution of AuNPs, thereby increasing nanoparticle-bacteria interactions. Upon contact with the bacterial cell envelope, surface-bound AuNPs can disrupt membrane integrity, increase membrane permeability, and promote the generation of reactive oxygen species (ROS), resulting in oxidative stress and leakage of intracellular constituents. These events subsequently interfere with essential biomolecules, including proteins and nucleic acids, ultimately leading to bacterial cell death (Slavin et al., 2017). The negligible antibacterial activity of GNFs alone, together with the marked inhibition observed for the AuNP-GNF composite, indicates that the antimicrobial activity is primarily attributed to immobilized AuNPs, while the nanofibrous scaffold functions as an effective carrier that enhances nanoparticle distribution and contact with bacterial cells. Similar antibacterial mechanisms have been proposed for AuNP-graphene-based nanocomposites intended for biomedical applications (Díez-Pascual, 2020; Duman et al., 2024).

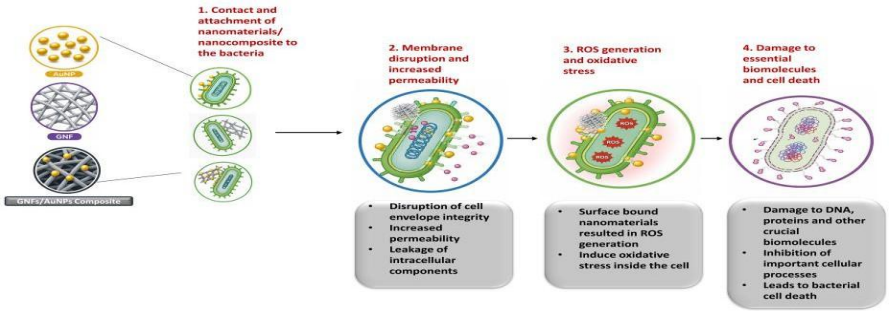

Figure 5. Schematic illustration of the proposed antibacterial mechanism of the AuNP-GNF composite.

3.8 DPPH free radical scavenging activity of AuNPs

For the evaluation of the antioxidant activity of the prepared AuNPs DPPH free radical scavenging assay at a concentration of 100 µg/mL (Fig. 5) was performed. The AuNPs displayed a 53 ± 0.7% DPPH radical scavenging activity, highlighting a moderate free radical scavenging capability in comparison to the standard

antioxidant.
The antioxidant activity of AuNPs could be correlated with their interaction with DPPH radicals and its ability of facilitating interfacial electron-transfer processes, which transforms DPPH into a more stable non-radical form (Razzaq et al., 2016). The scavenging activity observed is similar to other studies that have reported the DPPH radical-scavenging activity of citrate coated AuNPs; however, the activity levels may differ with the size of the nanoparticles, their surface chemistry, concentration, and the conditions of the assay (Shaabani et al., 2017). The results also emphasize the versatility of AuNPs, as they can have antioxidant and antibacterial properties (Khan et al., 2024).

4. CONCLUSION

In the current study, the GNFs and AuNPs were successfully synthesized by electrospinning and chemical reduction approach respectively, and subsequently utilized for AuNP–GNF nanocomposite fabrication. The formation of AuNPs was confirmed via physicochemical characterization with desirable surface, optical, and morphological characteristics, using FESEM and FTIR analyses that verified the successful synthesis of uniform graphene nanofibers as well as the successful incorporation of functional groups within the nanofibrous matrix. The synthesized AuNPs displayed concentration-dependent antibacterial potential against both Gram-negative and Gram-positive bacterial strains, whereas the GNFs alone showed negligible antibacterial potential. After the immobilization of AuNPs onto the GNFs the preserved antibacterial efficacy exhibiting enhanced antibacterial potential. Furthermore, the AuNPs displayed appreciable free radical scavenging capacity, showing their multifunctional potential. Collectively, these findings illustrate that the developed AuNP–GNF nanocomposite integrates the structural advantages of electrospun GNFs with the antioxidant and antimicrobial qualities of AuNPs, making it a suitable candidate for biomedical applications like wound dressings, antimicrobial coatings, and other infection-control strategies. Further examinations include biocompatibility assessment and in vivo evaluation that will simplify the translation of fabricated nanocomposite towards practical biomedical utilization.

REFERENCES

1. Asgari, S., Ziarani, G. M., Badiei, A., Setayeshmehr, M., Kiani, M., & Pourjavadi, A. (2022). Electrospun Ag-decorated reduced GO-graft-chitosan composite nanofibers with visible light photocatalytic activity for antibacterial performance. Chemosphere, 299, 134436.
2. Balouiri, M., Sadiki, M., & Ibnsouda, S. K. (2016). Methods for in vitro evaluating antimicrobial activity: A review. Journal of pharmaceutical analysis, 6(2), 71-79.
3. Batra, B., & Pundir, C. S. (2013). An amperometric glutamate biosensor based on immobilization of glutamate oxidase onto carboxylated multiwalled carbon nanotubes/gold nanoparticles/chitosan composite film modified Au electrode. Biosensors and Bioelectronics, 47, 496-501.
4. Bhattacharjee, S. (2016). DLS and zeta potential–what they are and what they are not?. Journal of controlled release, 235, 337-351.
5. Brand-Williams, W., Cuvelier, M. E., & Berset, C. L. W. T. (1995). Use of a free radical method to evaluate antioxidant activity. LWT-Food science and Technology, 28(1), 25-30.
6. Chung, E., Ren, G., Johnston, I., Matharu, R. K., Ciric, L., Walecka, A., & Cheong, Y. K. (2023). Applied methods to assess the antimicrobial activity of metallic-based nanoparticles. Bioengineering, 10(11), 1259.
7. Cui, Y., Zhao, Y., Tian, Y., Zhang, W., Lü, X., & Jiang, X. (2012). The molecular mechanism of action of bactericidal gold nanoparticles on *Escherichia coli*. Biomaterials, 33(7), 2327–2333. https://doi.org/10.1016/j.biomaterials.2011.11.057
8. Daniel, M. C., & Astruc, D. (2004). Gold nanoparticles: assembly, supramolecular chemistry, quantum-size-related properties, and applications toward biology, catalysis, and nanotechnology. Chemical reviews, 104(1), 293-346.
9. Díez-Pascual, A. M. (2020). Antibacterial action of nanoparticle loaded nanocomposites based on graphene and its derivatives: a mini-review. International Journal of Molecular Sciences, 21(10), 3563.
10. Duman, H., Akdaşçi, E., Eker, F., Bechelany, M., & Karav, S. (2024). Gold nanoparticles: multifunctional properties, synthesis, and future prospects. Nanomaterials, 14(22), 1805.
11. Fan, L., Dong, Y., Ismail, B. B., Zhang, L., Shi, Y., Wu, D., ... & Li, G. (2025). The antimicrobial activity and resistance evolution of nanomaterials: A review. ACS Materials Letters, 7(3), 1085-1111.
12. Fernández-Merino, M. J., Guardia, L., Paredes, J. I., Villar-Rodil, S., Solís-Fernández, P., Martínez-Alonso, A., & Tascón, J. M. D. (2010). Vitamin C is an ideal substitute for hydrazine in the reduction of graphene oxide suspensions. The Journal of Physical Chemistry C, 114(14), 6426-6432.
13. Frens, G. (1973). Controlled nucleation for the regulation of the particle size in monodisperse gold suspensions. Nature physical science, 241(105), 20-22.
14. Gao, Y., Kang, J., Tian, H., & Dong, A. (2025). Gold nanoparticle-based antibacterial materials and bioapplications. Soft Matter, 21(35), 6832-6851.
15. Gautam, A., Dabral, H., Singh, A., Tyagi, S., Tyagi, N., Srivastava, D., ... & Singh, A. (2024). Graphene-based metal/metal oxide nanocomposites as potential antibacterial agents: a mini-review. Biomaterials Science, 12(18), 4630-4649.

16. Hummers Jr, W. S., & Offeman, R. E. (1958). Preparation of graphitic oxide. Journal of the american chemical society, 80(6), 1339-1339.
17. Ibrahim, H. M., Reda, M. M., & Klingner, A. (2020). Preparation and characterization of green carboxymethylchitosan (CMCS)–Polyvinyl alcohol (PVA) electrospun nanofibers containing gold nanoparticles (AuNPs) and its potential use as biomaterials. International journal of biological macromolecules, 151, 821-829.
18. Ji, D., Lin, Y., Guo, X., Ramasubramanian, B., Wang, R., Radacsi, N., ... & Ramakrishna, S. (2024). Electrospinning of nanofibres. Nature Reviews Methods Primers, 4(1), 1.
19. Khan, S., Sher Khan, R., Khalid, A., Gul, M., Brekhna, Wadood, A., ... & Ullah, R. (2024). Biomedical and agricultural applications of gold nanoparticles (AuNPs): a comprehensive review. Zeitschrift für Physikalische Chemie, 238(8), 1383-1412.
20. Kumari, P., & Sharma, M. (2025). A Tyrosinase-Functionalized Graphene Nanofiber/AuNP Biosensor for Clinical Detection of Alkaline Phosphatase. Journal of the Indian Chemical Society, 102110.
21. Li, K. K., Hao, M., Kinoshita, S., & Xia, Y. (2024). Facile Synthesis and Characterization of Uniform Au Nanospheres Capped by Citrate for Biomedical Applications. Chemistry–A European Journal, 30(48), e202401144.
22. Marcano, D. C., Kosynkin, D. V., Berlin, J. M., Sinitskii, A., Sun, Z., Slesarev, A., ... & Tour, J. M. (2010). Improved synthesis of graphene oxide. ACS nano, 4(8), 4806-4814.
23. Martinov, B., Dimitrov, D., Foteva, T., Kostadinova, A., & Staneva, A. (2025). Structural Characterization, Cytotoxicity and Microbiological Activity of One-Step-Synthesized RGO/AuNPs Nanocomposites. Materials, 18(19), 4464.
24. Murray, C. J., Ikuta, K. S., Sharara, F., Swetschinski, L., Aguilar, G. R., Gray, A., ... & Tasak, N. (2022). Global burden of bacterial antimicrobial resistance in 2019: a systematic analysis. The lancet, 399(10325), 629-655.
25. Niżnik, Ł., Noga, M., Kobylarz, D., Frydrych, A., Krośniak, A., Kapka-Skrzypczak, L., & Jurowski, K. (2024). Gold nanoparticles (AuNPs)—toxicity, safety and green synthesis: a critical review. International journal of molecular sciences, 25(7), 4057.
26. Ozcicek, I. (2025). A critical review of in vitro and in vivo biomedical applications of gold nanoparticles: From toxicology to cancer therapy. Biomedicine & Pharmacotherapy, 190, 118410.
27. Pasieczna-Patkowska, S., Cichy, M., & Flieger, J. (2025). Application of Fourier transform infrared (FTIR) spectroscopy in characterization of green synthesized nanoparticles. Molecules, 30(3), 684.
28. Pei, S., & Cheng, H. M. (2012). The reduction of graphene oxide. Carbon, 50(9), 3210-3228.
29. Qin, Z., Fang, W., Jiang, Q., Li, J., & Zhang, H. (2024). The urchin-like gold nanoparticles/poly (ε-caprolactone)/chitosan electrospun nanofibers for antibacterial active packaging. International Journal of Biological Macromolecules, 274, 133287.
30. Raguindin, R. K. M., & Mercado, C. C. (2023). Localized surface plasmon resonance shift of biosynthesized and functionalized quasi-spherical gold nanoparticle systems. RSC advances, 13(35), 24211-24227.
31. Razzaq, H., Saira, F., Yaqub, A., Qureshi, R., Mumtaz, M., & Saleemi, S. (2016). Interaction of gold nanoparticles with free radicals and their role in enhancing the scavenging activity of ascorbic acid. Journal of Photochemistry and Photobiology B: Biology, 161, 266-272.
32. Sarma, P. P., Rai, A., & Baruah, P. K. (2024). Recent advances in the development of antibiotics-coated gold nanoparticles to combat antimicrobial resistance. Antibiotics, 13(2), 124.
33. Shaabani E, Amini SM, Kharrazi S, Tajerian R (2017). Curcumin coated gold nanoparticles: synthesis, characterization, cytotoxicity, antioxidant activity and its comparison with citrate coated gold nanoparticles. Nanomed J 4:115-125.
34. Slavin, Y. N., Asnis, J., Häfeli, U. O., & Bach, H. (2017). Metal nanoparticles: understanding the mechanisms behind antibacterial activity. Journal of nanobiotechnology, 15(1), 65.
35. Solanki, R., Makwana, N., Kumar, R., Joshi, M., Patel, A., Bhatia, D., & Sahoo, D. K. (2024). Nanomedicines as a cutting-edge solution to combat antimicrobial resistance. RSC advances, 14(45), 33568-33586.
36. Turkevich J, Stevenson PC, Hillier J. 1951. A study of the nucleation and growth processes in the synthesis of colloidal gold. Discussions of the Faraday Society. 11:55–75.
37. Wang, A., Ng, H. P., Xu, Y., Li, Y., Zheng, Y., Yu, J., ... & Fu, L. (2014). Gold nanoparticles: Synthesis, stability test, and application for the rice growth. Journal of Nanomaterials, 2014(1), 451232.
38. Wang, C., Su, Y., & Xie, J. (2024). Advances in electrospun nanofibers: versatile materials and diverse biomedical applications. Accounts of Materials Research, 5(8), 987-999.
39. Yang, X., Yang, J., Wang, L., Ran, B., Jia, Y., Zhang, L., ... & Jiang, X. (2017). Pharmaceutical intermediate-modified gold nanoparticles: against multidrug-resistant bacteria and wound-healing application via an electrospun scaffold. ACS nano, 11(6), 5737-5745.
40. Zhang, P., Hou, H., Xu, S., Wen, Y., Zhang, Y., & Xing, F. (2025). Localized surface plasmon resonance sensing based on monometallic gold nanoparticles: from material preparation to detection of bioanalytes. Analytical Methods, 17(5), 892-915.